Preprint
UCRL-JC-135852 Rev. 1

Comparison of the Crevice Corrosion Resistance of Alloys 625 and C22

B.A. Kehler, G.O. Ilevbare and J.R. Scully

This article was submitted to
196th Meeting of the Electrochemical Society
Honolulu, HI
October 17-22, 1999

November 11, 1999

U.S. Department of Energy
Lawrence
Livermore
National
Laboratory

COMPARISON OF THE CREVICE CORROSION RESISTANCE OF ALLOYS 625 AND C22

B.A. Kehler, G.O. Ilevbare, J.R. Scully
Center for Electrochemical Science and Engineering
Department of Materials Science and Engineering
University of Virginia
Thornton Hall, Charlottesville, VA 22903-2442

ABSTRACT

The effects of electrolyte composition and oxide film age on the crevice corrosion properties of alloys 625 and C22 were studied at 95°C. Critical potentials were determined using conventional current density thresholds. Crevice stabilization potentials are influenced by the bulk electrolyte composition, oxide properties, and alloy dissolution behavior. Repassivation and deactivation potentials are controlled by the chemistry of the crevice solution, mass transport considerations, and the electrochemical properties of the alloys. Critical potential data also showed the large influence of air formed oxide film age on stabilization. Air aged C22 specimens exhibited the highest resistance to crevice corrosion in terms of critical crevice potentials, while freshly polished C22 exhibited the lowest resistance.

INTRODUCTION

The Yucca Mountain Site Characterization Project is concerned with the corrosion resistance of candidate engineered waste package materials. Researchers have proposed a variety of waste package designs for US and Canadian High Level Nuclear Waste Repositories. A common feature of each design is the possibility of utilizing a corrosion resistant material (CRM) such as a nickel-based super alloy or titanium-based alloy. A suitable CRM may provide kinetic immunity if the combination of repository environmental conditions and alloy resistance assures a passive condition with negligible chance of localized corrosion stabilization as well as low enough passive dissolution rates to ensure conventional corrosion allowance over geological times. The CRM may also provide a second form of corrosion allowance, if it can be scientifically demonstrated that a mechanism for stifling of localized corrosion sites occurs well before waste canisters are penetrated. Lastly, a suitable CRM may provide a low probability of initiation and continued propagation such that a tolerable degree of waste package penetration occurs.

Unfortunately, a large database on the crevice corrosion properties of C22 does not exist in comparison to 625. Alloy screening tests in oxidizing acids containing $FeCl_3$ indicate that C22 is more resistant to crevice corrosion than 625 as indicated by critical pit and crevice propagation temperatures (1). Important differences in alloy compositions as expressed by pitting resistance equivalency numbers support these findings. This study seeks to compare 625 and C22 on the basis of critical potentials. Future studies will use this critical potential data to guide experiments on metastable breakdown-repair events that may lead to crevice stabilization.

PROCEDURES

Alloy 625 (UNS No. N06625) in a mill-annealed condition and alloy C22 (UNS No. N06022) in a solution-annealed condition were studied to determine the effects of electrolyte composition and oxide properties on crevice corrosion. Alloy compositions and properties are shown in Tables I and II. Specimens were tested with surfaces in either a freshly polished or a laboratory air aged condition. The face of the sample was placed inside a crevice assembly consisting of ceramic multiple crevice formers lined with polytetrafluoroethylene (PTFE) tape. The torque applied was 70 in-lb. This arrangement created a reproducible tight crevice. Experiments were conducted at 95°C in 5 M LiCl electrolytes at pH levels of 2.75 and 7.75. Sodium sulfate and sodium nitrate were added in concentrations to yield electrolytes with ratios of chloride ions to total oxyanions of 10:1 and 100:1. The total wetted area was approximately 7.8 cm^2. The open circuit potential was allowed to stabilize at testing temperature for approximately one to three hours prior to polarization. Cyclic potentiodynamic polarization scans were performed using a polarization rate of 0.05 mV/sec starting at 50 mV below the open circuit potential. The electrode potential was measured with respect to a Ag/AgCl (saturated KCl) electrode held at room temperature. The potential at which the current permanently exceeded 10^{-6} A/cm^2 on the forward scan was selected as a threshold to define the critical crevice potential, E_{crev}. Two current threshold criteria were used to define the repassivation potential, $E_{r,crev}$ (10^{-5} and 10^{-6} A/cm^2). Other electrochemical tests were performed to distinguish localized corrosion from Cr (Mo, Ni) transpassivity.

RESULTS

Stoichiometry of Alloy Dissolution during Crevice Corrosion

The active dissolution process during crevice corrosion was explored through comparison of mass loss after crevice corrosion to experimentally measured dissolution charge. The dissolution process was assumed to generate Ni^{2+}, Cr^{3+}, Fe^{2+}, Mo^{3+}, and W^{4+} in direct proportion to the composition of each alloy. Equivalent weights for 625 and C22 were calculated (ASTM G-102) assuming that each element was oxidized during crevice attack and that there was no preferential dissolution. The calculated equivalent weight range for 625 was 26.62-26.82 grams/eq, whereas the range for C22 was 26.18-26.43 grams/eq. Figure 1 shows faradaic mass loss (calculated using the mid-range values of the calculated equivalent weights) versus gravimetric mass loss.

Critical Potentials for Crevice Stabilization and Repassivation

Critical potentials were determined from slow scan polarization data on specimens containing multiple crevice assemblies using the 10^{-6} A/cm^2 threshold current. A 10^{-5} A/cm^2 threshold was also used for determination of $E_{r,crev}$. Figure 2 illustrates examples for 625 and C22. The slope of the E-log i region just after crevice stabilization was almost always steeper in the case of C22. The large sustained increase in current above E_{crev} is likely associated with stabilization of sites similar to or the same as metastable crevice sites rather than initial atomistic-scale breakdown. Metastable crevice corrosion events can be observed as small current spikes at potentials significantly below those at which crevice stabilization took place. Figure 3 shows a comparison of these events in the passive regions of both alloys. Examination of the passive regions illustrates a higher number of metastable events for 625 than for C22. The events grew to higher peak currents and more charge was passed in the events on 625 as compared to C22.

Additional experiments on 625 and C22 in 5 M Cl^- electrolyte at ratios of 100:1 and 10:1, respectively, showed the independence of repassivation potential and accumulated dissolution charge. Figure 4 illustrates that $E_{r,crev}$ is independent of charge over the range from zero to 1000 coulombs/cm^2 for 625 and zero to 40 coulombs/cm^2 for C22. The range of accumulated charge is much smaller for C22 due to slower crevice corrosion propagation rates.

Effect of Solution Composition on Critical Potentials

The effect of the electrolyte ratio on crevice corrosion was explored for each alloy. The results for 625 are shown in Figure 5 for pH 2.75 and 7.75. The data are reported as the cumulative probability for achieving a given critical potential as pioneered by Shibata (2). It should be noted that a linear cumulative probability plot indicates a normal distribution (ASTM G-16) (2, 3). Moreover, a steeper curve indicates less data variability. Both pH levels are seen to produce statistically similar values of E_{crev} and $E_{r,crev}$. Therefore, these critical potentials are found to be independent of the bulk solution pH over the range explored. It also can be seen that $E_{r,crev}$ is only slightly affected by the initial chloride/oxyanion ratio. A slightly lower median value is seen for the 100:1 ratio at each pH. In contrast, E_{crev} is more strongly affected by the ratio in electrolyte compositions. Specifically, E_{crev} is lowered when the ratio is greater. Figure 5 also shows that there is little distinguishable difference between the critical potentials of freshly polished versus air aged 625 samples. However, more data is required.

The results for C22 are shown in Figure 6 for pH 2.75 and 7.75. It can be seen that the distribution for E_{crev} is shifted to more noble potentials for electrolyte ratios of 10:1 and that there is little effect of bulk pH. Also, critical crevice potentials for air aged specimens are shifted to even more noble values than freshly polished specimens for comparable conditions. The initial solution composition had only a small effect on the repassivation potentials with median values for the 100:1 ratio shifted to slightly more negative potentials than the 10:1 ratio.

Comparison of Alloys 625 and C22

Figure 7 presents a comparison of the critical potentials for 625 and C22 in the pH 7.75 (10:1) electrolyte. $E_{r,crev}$ was found to be statistically similar for both alloys at the 10^{-6} A/cm^2 threshold, but slightly more positive median potentials were observed for C22 at the 10^{-5} A/cm^2 threshold. In addition, there is less data variability indicating that $E_{r,crev}$ is a highly reproducible parameter. In contrast, the results for E_{crev} were more complex. Here it was observed that freshly polished C22 specimens were actually less resistant to crevice stabilization than either freshly polished or air aged 625 specimens as indicated by a more negative median E_{crev}. However, air aged C22 specimens exhibited the greatest values of E_{crev}. In fact, a percentage of the air aged C22 specimens tested in the 10:1 solution did not initiate crevice corrosion but instead experienced increases in anodic current attributed to transpassivity. Similar trends for critical crevice potentials and repassivation potentials were seen with the other solution compositions.

DISCUSSION

Crevice Dissolution Rates

Because crevice surface potentials during crevice corrosion precluded hydrogen evolution, separation of anode and cathode was nearly 100% at potentials above the repassivation potential. Therefore, nearly 100% of dissolution charge was recorded. Figure 1 shows the relationship between faradaic and gravimetric mass loss. A slope of one for the linear regression of the data would indicate that the assumption of stoichiometric dissolution is valid. Figure 1 shows that this assumption is valid for C22. However, the assumption is not accurate for 625, possibly indicating the preferential dissolution of nickel, molybdenum, or iron. Figure 1 also shows that the range of mass losses for 625 was far greater than for that of C22 although the range of testing times for C22 was higher. Dissolution rate can also be seen in the form of the E-log i slope in the range of stable crevice corrosion from a polarization curve (Figure 2). A steeper E-log i slope for the upward scan during crevice attack indicates that either fewer additional sites were initiated and stabilized above E_{crev} or that the growth rate of a fixed number of sites initiated at an earlier time was slower. A flatter E-log i slope, typical of 625, is indicative of more rapid dissolution kinetics per unit area or a more rapid increase in the area associated with crevice corrosion during the forward potential scan. Also, more frequent metastable events increase the possibility of forming more stable crevice sites because of thin oxide films at the metastable sites (4) and the greater number of such sites available for stabilization (Figure 3). Optical microscopy characterization after completion of potential scans indicated that crevice attack was restricted to the crevice area just under

crevice formers in the case of C22. In contrast, crevice corrosion of 625 occurred beneath the crevice but extended outside of the area of the tight crevice defined by the ceramic washer and deformable tape insert. This is indicative of a less concentrated critical crevice solution for depassivation of 625. Lillard, et al. (5) showed through tests in simulated crevice environments that increasing Mo content leads to lower passive current densities and lower peak active current densities. Therefore, because C22 has a higher Mo content than 625, any dilution of the critical crevice solution will likely promote the cessation of crevice attack.

Repassivation Potentials

Two types of $E_{r,crev}$ can be observed depending on experimental conditions (6). The first is associated with the potential at which crevice dissolution and cation hydrolysis do not occur at fast enough rates to maintain a depassivating crevice solution within the crevice. This potential is thus associated with a lowering of the crevice dissolution rate to eventually enable cessation of crevice attack because the depassivating crevice solution is not maintained. This potential will be dependent upon time, crevice geometry (i.e., depth and, therefore, dissolution charge), temperature, solution composition, and dissolution rate. The first four factors control the mass transport properties of the crevice solution, while the dissolution rate controls the rate of hydrolyzable cation production. Repassivation on reverse potential scans will hence be indicated by re-establishment of passivity at some characteristic critical potential where the dissolution rate becomes slower than the transport rate leading to dilution of the crevice solution and an increase of the crevice pH. Therefore, this potential is not determined solely by material properties. Unfortunately, potential sweep rate can confound determination of this potential when all other variables are fixed since a fast sweep rate will enable crevice corrosion to be momentarily sustained at a lower potential and, hence, lower crevice corrosion rate than sustainable given infinite time. The passive current density is also observed to be greater on the reverse scan compared to the initial scan because the newly reformed oxide over crevice sites is thin, defective, and supports cation transmission at higher rates. Moreover, the solution is acidified from cation hydrolysis and passive current density over all passivated surfaces is strongly effected by pH (5, 7). These factors can confound determination of $E_{r,crev}$ associated with repassivation. This $E_{r,crev}$ is most likely observed upon slow downward scanning or long holds during downward potential stepping (8). A high current threshold of 10^{-5} A/cm^2 was selected to explore repassivation because it could be argued that a lower current density could be attributed to passive dissolution.

The second type of $E_{r,crev}$ value is associated with the open circuit potential of the actively corroding crevice. Below this potential, the electrochemical reactions at the crevice become net cathodic. This potential, sometimes referred to as a deactivation potential, is not necessarily associated with repassivation. This potential will be indirectly dependent on crevice geometry because it affects the pit chemistry that can develop, but is more directly governed by the preexisting pit chemistry, temperature, and

alloy electrochemical dissolution properties. This latter type of $E_{r,crev}$ will most likely be observed upon fast scan rate as seen elsewhere (9) because the concentrated crevice solution composition has little time to become diluted at rapid scan rates. It is usually the most conservative of the two values of $E_{r,crev}$ because it is often associated with more negative potentials (9). Caution is necessary, however, since this potential can be corrupted by prior crevice corrosion if induced at very high potentials. The Cr^{6+} and Mo^{6+} species generated at such high potentials are oxidizers that positively shift the crevice OCP more than is possible from just protons and lower valence state metal cations. This was observed in the studies of Cragnolino on C22 (10), but has been carefully avoided in this study by staying below applied potentials associated with transpassivity when $E_{r,crev}$ was investigated. Note that the 10^{-6} A/cm^2 threshold does not, in and of itself, discriminate between these two types of $E_{r,crev}$ and either one could theoretically be observed in a given test. However, $E_{r,crev}$ near 10^{-6} A/cm^2 was most likely of the second type since crevice corrosion often became net cathodic at potentials near this current threshold. Thus, $E_{r,crev}$ at 10^{-6} A/cm^2 is likely associated with deactivation and is a conservative lower bound, while that obtained at 10^{-5} A/cm^2 at slow scan rate is more representative of repassivation and presents an upper bound. Figures 5 and 6 illustrate $E_{r,crev}$ data using the 10^{-6} A/cm^2 current threshold. The distributions for $E_{r,crev}$ are not as widely separated as the distributions for E_{crev} indicating that the bulk solution composition affects crevice stabilization but does not affect the deactivation potential. $E_{r,crev}$ is slightly greater for C22 at 10^{-5} A/cm^2.

Repassivation potential has also been shown to be dependent upon the total anodic charge collected (9, 11). However, such a dependency is more likely when the first definition of $E_{r,crev}$ applies because the mass transport properties of the crevice are more heavily influenced by crevice depth (and, therefore charge) compared to the OCP of an active crevice assuming the crevice solution composition has not become diluted. Also, Yashiro and Tanno have shown that $E_{r,crev}$ is independent of accumulated charge on AISI 304 stainless steel when the electrolyte chloride concentration is above 0.5 M (11). The lack of correlation between repassivation potential and charge density as shown in Figure 4 allowed for the unique determination of $E_{r,crev}$ without concern for accumulated charge. Data for both pH values were shown because it was determined that bulk solution pH has no effect on critical potentials for the pH range examined.

Oxide Aging

Shibata and Takamiya showed that oxide aging shifts the critical pitting potentials of Mo containing stainless steels to more noble values (4). Oxide thickness has been shown to increase logarithmically on nickel and iron (12). Moreover, aging decreases the defect concentration in the oxide film even after thickness reaches a steady state (13, 14). Figure 6 shows that there is a shift in the distribution of crevice potentials to more noble values for air aged C22 as compared to freshly polished C22. However, this effect is not seen for 625 (Figure 5). Therefore, oxide properties and consequently, aging, may have a

greater effect on the crevice corrosion resistance of C22 than of 625. Differences in E_{crev} on C22 with oxide aging are speculatively attributed to either differences in oxide film thickness or the extent of oxide defects present in the freshly polished material. A less defective and thicker oxide would have the effect of elevating the value of E_{crev}. The notion that an air aged oxide increases E_{crev} is supported by the OCP data of this study and the literature (4).

CONCLUSIONS

Crevice corrosion properties of alloys 625 and C22 at 95°C are clearly influenced by electrolyte compositions. Crevice stabilization occurred at more active potentials in electrolytes with a ratio of chloride to total oxyanions of 100:1 as compared to 10:1. Bulk pH is not as influential in the process of crevice stabilization. Repassivation potentials are similar for both alloys and are not influenced by the electrolyte composition or accumulated anodic charge. Air aged C22 specimens exhibited more noble stabilization potentials as compared to freshly polished C22 specimens. However, this effect was not noted on 625. Further studies are necessary to determine the important features of oxide films (i.e., structure, thickness, or the effect of aging on defects) that affect crevice stabilization.

ACKNOWLEDGEMENTS

This work was performed under the auspices of the U.S. Department of Energy by Lawrence Livermore National Laboratory under contract W-7405-ENG-48. This work is supported by Yucca Mountain Site Characterization Project, LLNL. The authors would also like to thank EG&G Princeton Applied Research and Scribner Associates for their ongoing technical support to the Center for Electrochemical Science and Engineering at the University of Virginia.

REFERENCES

1. E.L. Hibner, CORROSION/86, Paper No. 181, NACE, Houston, TX (1986).
2. T. Shibata and T. Takayama, Corrosion Science, 33, 243 (1977).
3. M. Kowaka, Introduction to Life Prediction of Industrial Plant Materials: Application of the Extreme Value Statistical Method for Corrosion Analysis, p. 75, Allerton Press, Inc., New York (1994).
4. T. Shibata and H. Takamiya, in Critical Issues in Reducing the Corrosion of Steels/1985, H. Leidheiser, Jr. and S. Haruyama, Editors, p. 17, The National Association of Corrosion Engineers Proceedings Series, Houston, TX (1986).

5. R.S. Lillard, M.P. Jurinski, and J.R. Scully, Corrosion, 50, 251 (1994).
6. G.S. Frankel and J.R. Scully, J. Electrochem. Soc., 143, 1834 (1996).
7. R.W. Evitts, M.M.A. Gad, M.K. Watson, and J. Postlethwaite, CORROSION/93, Paper No. 601, NACE, Houston, TX (1993).
8. D. Dunn and N. Sridhar, in Critical Factors in Localized Corrosion II/95, P.M. Natishan, R.G. Kelly, G.S. Frankel, and R.C. Newman, Editors, PV 95-15, p. 79, The Electrochemical Society Proceedings Series, Pennington, NJ (1995).
9. N. Sridhar and G.A. Cragnolino, Corrosion Science, 49, 885 (1993).
10. G.A. Cragnolino, Waste Package Degradation Expert Elicitation Workshop, February 2, 1998.
11. H. Yashiro and K. Tanno, Corrosion Science, 31, 485 (1990).
12. B. MacDougall and M.J. Graham, in Corrosion Mechanisms in Theory and Practice, P. Marcus and J. Oudar, Editors, p. 153, Marcel Dekker, Inc., New York (1995).
13. B. MacDougall and M. Cohen, J. Electrochem. Soc., 124, 1185 (1977).
14. B. MacDougall, D.F. Mitchell, and M.J. Graham, Isr. J. Chem., 18, 125 (1979).
15. A.J. Sedriks, Corrosion of Stainless Steels, p. 47, John Wiley & Sons, New York (1996).

Table I. Chemical composition (weight percent) of 625 and C22.

Element	Alloy 625	Alloy C22
C	0.03-0.023	0.005-0.007
Cr	20.59-21.56	21.52-21.58
Co	0.05-0.09	0.44-1.69
Fe	3.40-3.82	3.75-3.90
Mn	0.06-0.11	0.20-0.24
Mo	8.81-8.95	12.79-13.30
Ni	Balance	Balance
P	0.005-0.008	0.005-0.009
Si	0.09-0.34	0-0.01
S	0.0003-0.004	0.001-0.002
W	-	2.79-2.85
V	-	0.13-0.16
Al	0.18-0.20	-
Cb+Ta	3.36-3.369	-
Ti	0.26	-

Table II. Alloy Cr equivalency, pitting resistance equivalency number, heat treatment, and hardness.

	625	C22
Cr Equivalency	49.16-50.33	61.57-62.75
PREN	49.66-51.10	63.79-65.46
Heat Treatment	Mill Annealed (871°C)	Solution annealed (1121°C)
Hardness (HRB)	96-97	91-92

PREN = wt.%Cr + 3.3wt.%Mo + 16wt.%N (15)
Cr Equivalency = wt.%Cr + 1.6wt.%Mo + 4.3wt.%Nb + 7wt.%W (5)

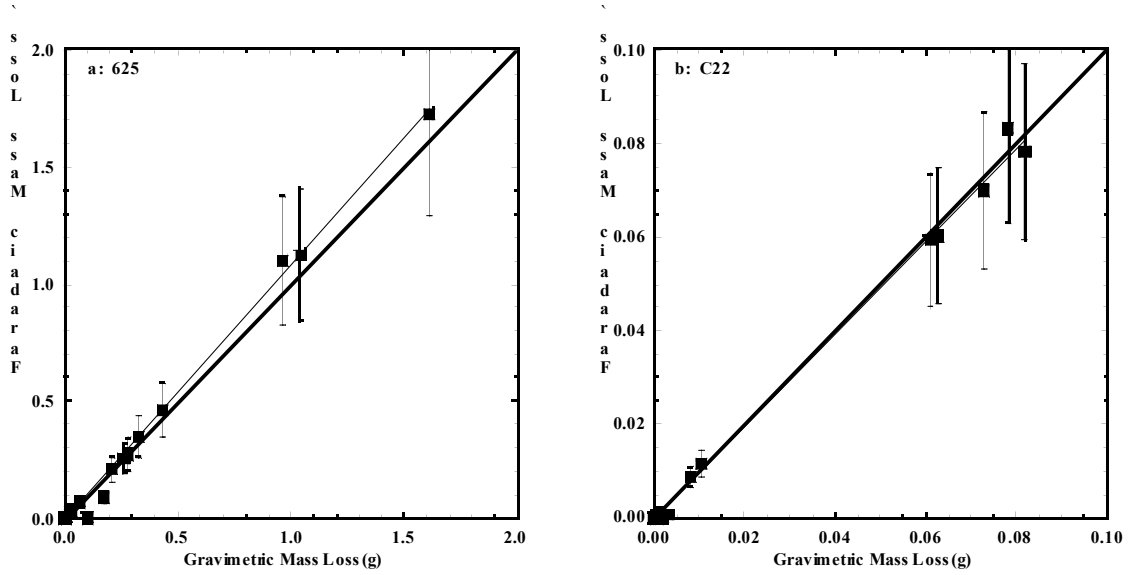

Figure 1. Faradaic versus gravimetric mass loss for 625 (a) and C22 (b) assuming stoichiometric dissolution and equivalent weights of 26.72 g/eq and 26.31 g/eq for 625 and C22, respectively. The cases of 30 g/eq and 20 g/eq are indicated by the upper and lower bars, respectively. The plot diagonal has a slope of one and is shown as a comparison to the experimental data.

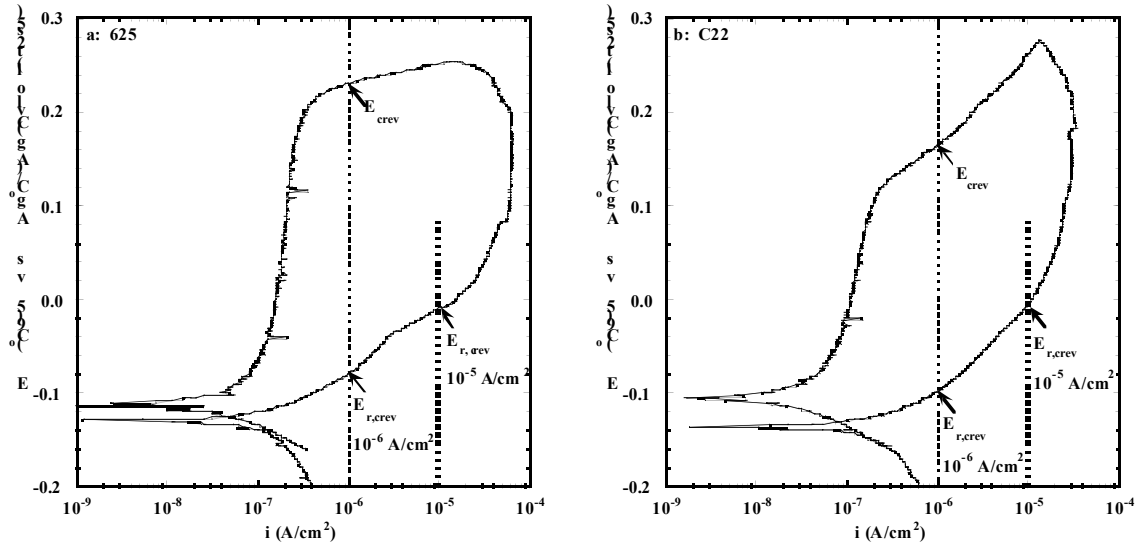

Figure 2. Cyclic polarization curves showing critical potentials for 625 (a) and C22 (b) in a pH 7.75 (10:1) electrolyte.

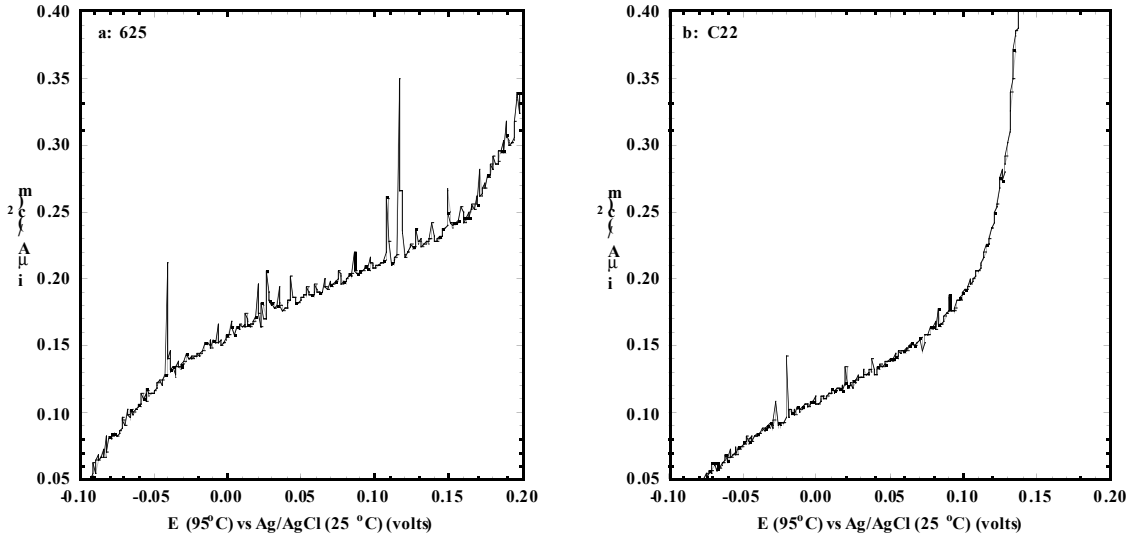

Figure 3. Passive region of the cyclic polarization curves for 625 (a) and C22 (b) shown in Figure 2. The small current spikes indicate metastable events.

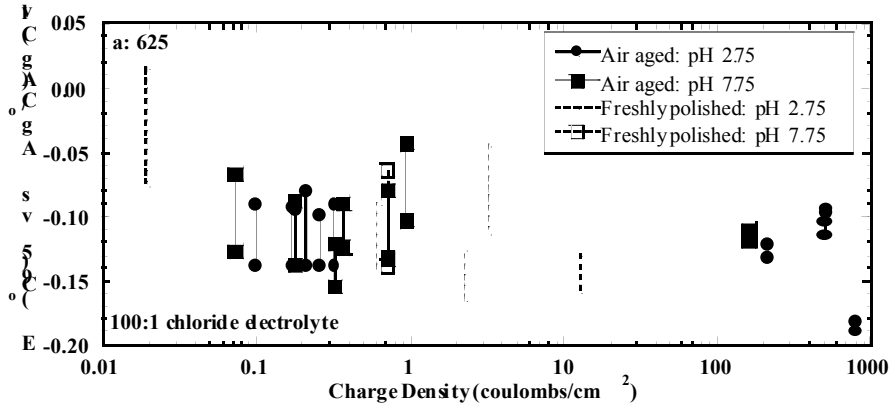

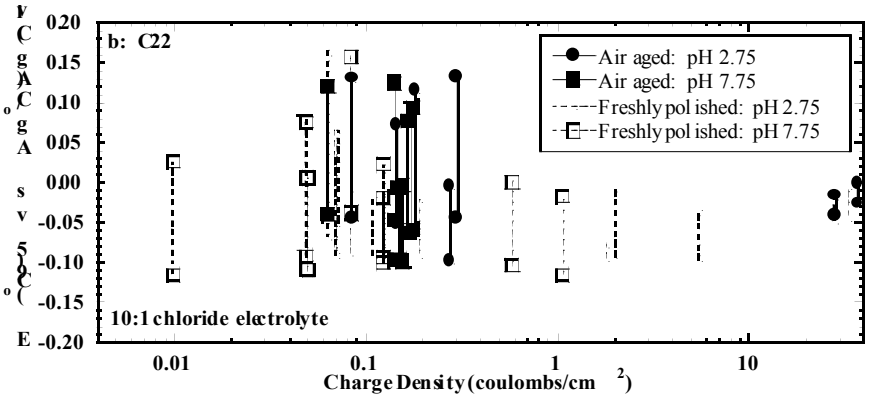

Figure 4. Repassivation potential as a function of charge density for 625 (a) and C22 (b). The upper and lower bounds are determined by current thresholds of 10^{-5} and 10^{-6} A/cm^2, respectively. Note that data is included for both pH values because it has been determined that critical potentials are nearly independent of bulk pH.

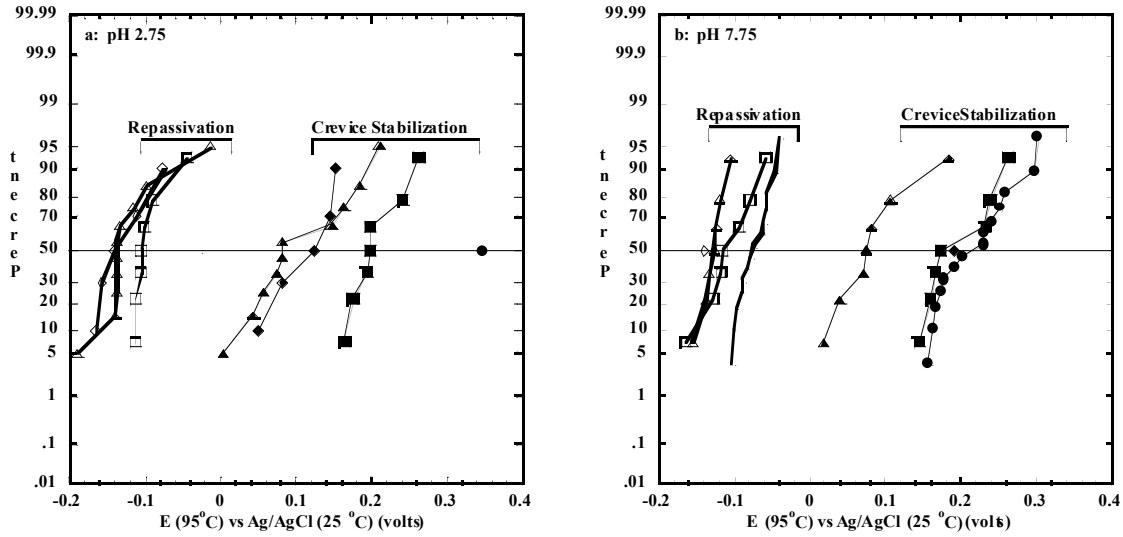

Figure 5. Cumulative probability plot of critical potentials for 625 in pH 2.75 (a) and pH 7.75 (b) electrolyte. Repassivation potentials are determined using the 10^{-6} A/cm^2 current threshold (!E_{crev}: freshly polished (10:1), "$E_{r,crev}$: freshly polished (10:1), #E_{crev}: air aged (10:1), Q$E_{r,crev}$: air aged (10:1), øE_{crev}: freshly polished (100:1), Ø$E_{r,crev}$: freshly polished (100:1), pE_{crev}: air aged (100:1), r$E_{r,crev}$: air aged (100:1)).

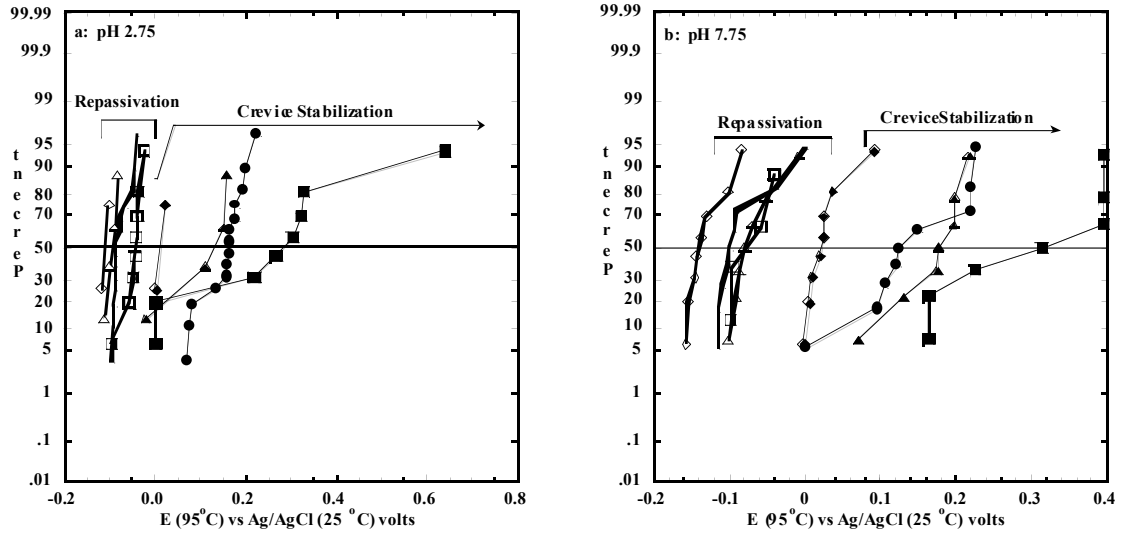

Figure 6. Cumulative probability plots of critical potentials for C22. $E_{r,crev}$ is determined using the 10^{-6} A/cm^2 current threshold (!E_{crev}: freshly polished (10:1), "$E_{r,crev}$: freshly polished (10:1), #E_{crev}: air aged (10:1), Q$E_{r,crev}$: air aged (10:1), øE_{crev}: freshly polished (100:1), Ø$E_{r,crev}$: freshly polished (10:1), pE_{crev}: air aged (100:1), r $E_{r,crev}$: air aged (100:1)).

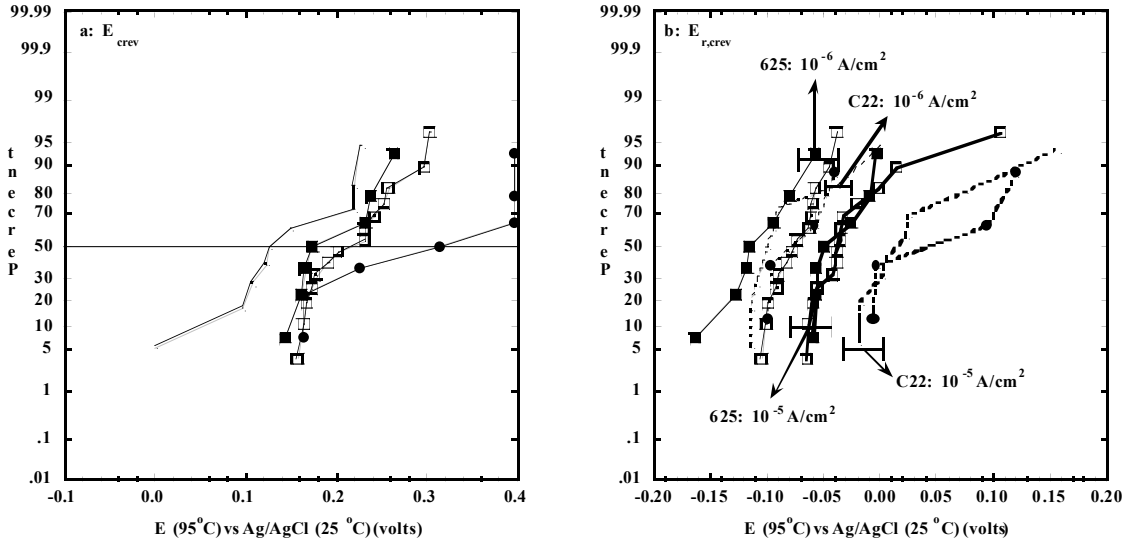

Figure 7. Cumulative probability plots comparing E_{crev} (a) and $E_{r,crev}$ (b) of 625 and C22 in a pH 7.75 (10:1) electrolyte. In (b) current thresholds of 10^{-6} and 10^{-5} A/cm^2 are represented by thick and thin lines, respectively (QFreshly polished 625, "Freshly polished C22, #Air aged 625, !Air aged C22).